Compact Tri-band Wilkinson Power Divider Based on Metamaterial Structure for Bluetooth, WiMAX, and WLAN Applications

Farzad Khajeh-Khalili[a], M. Amin Honarvar[a*], Abdolmehdi Dadgarpour[b], Bal S. Virdee[c], and Tayeb A. Denidni[b]

[a]Department of Electrical Engineering, Najafabad Branch, Islamic Azad University, Najafabad, Iran
[b]Institut National de la Recherche Scientifique, INRS-EMT, University of Quebec, Montreal, Canada
[c]Center for Communications Technology, London Metropolitan University, London, UK
*Corresponding author: Amin.Honarvar@pel.iaun.ac.ir

A novel Wilkinson power divider is presented in this paper for triple band operation. It comprises a Π-shaped transmission-line coupled to a rectangular split ring resonator metamaterial structure. The μ-negative feature of the rectangular split ring resonator metamaterial structure is investigated by retrieving its constitutive parameters from the S-parameter response. To demonstrate the versatility of the proposed Wilkinson power divider it was designed to cover Bluetooth (2.4 GHz), WiMAX (3.5 GHz), and WLAN (5.2 GHz). The tri-band Wilkinson power divider was fabricated and its performance measured to verify the design. Good agreement between the measured and simulated data is obtained. Measured results show that the tri-band Wilkinson power divider has fractional bandwidth of 3.86%, 5.82%, and 3.89% at 2.4, 3.5, and 5.2 GHz, respectively. In addition, the rectangular split ring resonator metamaterial Wilkinson power divider has a small physical footprint (14 mm ×17.9 mm or $0.15\lambda_g \times 0.19\lambda_g$), which is 60% smaller than conventional designs.
Keywords: Wilkinson power divider; Rectangular split ring resonator; Metamaterial; Negative permeability

1. Introduction

The original power divider developed by Wilkinson, which operates in a single band, is an important component for microwave systems for power division. Power dividers are used in various microwave circuits, such as mixers, balanced amplifiers, and antenna array. Conventional equal and unequal power-dividing ratio Wilkinson power dividers (WPD) consist of two quarter-wavelength lines with the same and different characteristic impedances, respectively, at the design frequency. The main challenge facing conventional WPD is its large circuit size, especially at low microwave frequencies, and limited bandwidth due to the use of a pair of quarter-wavelength transmission-lines (TLs) in its design [1]. With the advent of multi-band wireless communication systems, a lot of studies have been done over the recent years on developing multi-band WPD [2-10]. In addition, wideband and ultra wideband WPDs using innovative methods have been reported [11-14].

In [2], a dual-band WPD is proposed using a two-section TL transformer with its output ports connected through a parallel *RLC* circuit to improve the isolation at the two bands. In [3], a novel dual-band WPD is presented using the model of Π-shaped TL in place of the common quarter-wavelength TL. In [4], the isolation between the output ports is improved by inserting a complex isolation component across the two quarter-wavelength TLs at an arbitrary phase angle from the input terminal; however, this design is band limited. Three-section TL transformer is used to design a tri-band WPD in [5]. The operating frequencies of this WPD are 0.9 GHz, 1.17 GHz, and 2.43 GHz. The important point is that the dimensions of this structure are 1705 mm^2.

In [6] a quad-band WPD consists of three TLs and two loaded shorted-stubs. Although the above designs have good isolation between their output ports, their dimensions are relatively large for today's multi-band communication systems.

More recently, the designs of WPDs have become more compact [15-19]. For example, in [15] the WPD is proposed using two section asymmetrical T-structures to achieve a significant size reduction. The asymmetrical T-structure is realized by two series high-impedance lines with unequal electrical lengths and a shunt low-impedance line. Although these designs are compact in size, their bandwidth is limited. Also, metamaterial structures have been used to design WPDs with multi-band response [20-23], however the dimensions of these structures are relatively large for practical applications. It should be noted that in [24], we have designed a novel compact wideband triple lines WPD using particle swarm optimization (PSO) technique which operates from 0.5 to 4.5 GHz for application in several wireless communication standards. This WPD has small dimensions and good bandwidth. Now, the idea is to design a multi-band WPD using metamaterial structures.

In this paper, a compact novel tri-band WPD is designed, simulated, and fabricated. The proposed WPD is composed of a Π-shaped TL coupled to a metamaterial structure, which is based on a rectangular split ring resonator metamaterial (RSRRM). The WPD is designed to operate at 2.4, 3.5, and 5.2 GHz corresponding to Bluetooth, WiMAX, and WLAN bands, respectively. Measured results are used to validate the design. The proposed tri-band WPD is 60% smaller than its conventional counterpart reported in [5].

2. Design Structure

This section gives a generalized three-step design process for RSRRM-WPD. The proposed WPD is shown in Figure 1. As can be seen, this WPD consists of the RSRRM unit cells and Π-shaped structures sections. The 50 Ω input and output ports are attached to SMA connectors. The final dimensions, shown in Figure 1, are: x=14, y=17.9, t=4.6, w=0.25, z=0.6, v=2.2, and Gap=0.6 (all in millimeters). In this work, CST Microwave Studio 2017 is used to simulate WPD structures on a Taconic substrate with relative permittivity of 2.65, tan δ=0.002, and thickness of h=0.8 mm.

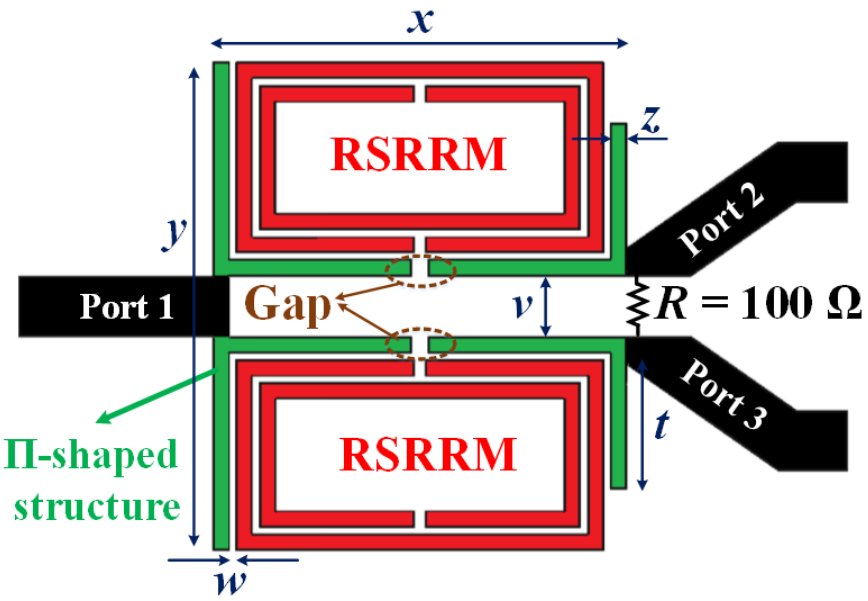

Figure 1. The proposed RSRRM-WPD.

a. Step 1: Design of a Dual-band WPD for Bluetooth and WLAN (2.4 / 5.2 GHz)

Figure 2a shows the schematic diagram of the conventional WPD that consists of two quarter wave-length transformers with Z_1=70.71 Ω and an isolation resistor R=100 Ω [1]. To reduce the area of the conventional WPD with dual-band performance, a Π-shaped structure, shown in Figure 2b, is chosen to realize the quarter-wavelength transformers. This structure consists of a series TL with an electrical length of θ_2 and characteristic impedance of Z_2, connected to a pair of open circuit stubs (Z_3, θ_3) [7].

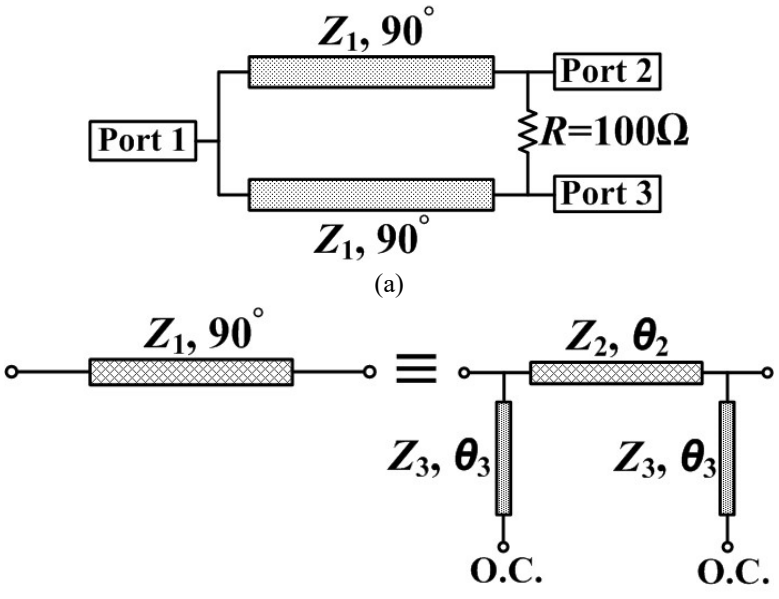

Figure 2. (a) Conventional WPD and (b) equivalent circuit for the quarter-wavelength.

The Π-shaped structure in Figure 2b can be represented by ABCD matrix. By equating the ABCD matrix of the quarter-wavelength TL to the ABCD matrix of the Π-shaped structure results in the following relations:

$$Z_2 = Z_1 \csc(\theta_2); \qquad \text{where } \theta_2 = \frac{n\pi}{1+f_2/f_1}, \quad n = 1,2,... \tag{1}$$

$$Z_3 = Z_2 \tan(\theta_2)\tan(\theta_3); \qquad \text{where } \theta_3 = \frac{m\pi}{1+f_2/f_1}, \quad m = 1,2,3,... \tag{2}$$

In relations (1) and (2), θ_2 and θ_3 are the electrical lengths of the series and shunt elements, respectively, of the Π-shaped structure at the two operating frequencies f_1 and f_2. For size reduction, n=m=1 is selected. The two operating frequencies are chosen to be f_1=2.4 GHz and f_2=5.2 GHz (f_2/f_1=2.16). The impedance and electrical length of the stubs in the Π-shaped structure were calculated using Equations (1) and (2) to be Z_2=99 Ω and Z_3=103 Ω. Figure 3 shows S_{11} (return-loss) parameter of the dual-band WPD. Inset in Figure 3 is the schematic configuration of the proposed dual-band WPD.

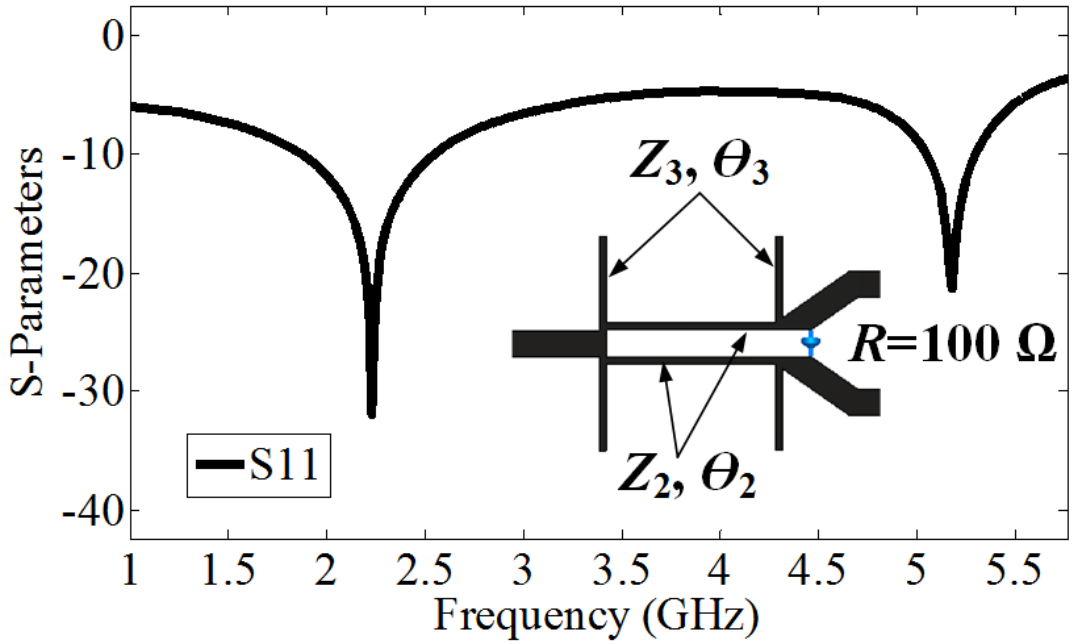

Figure 3. S_{11} response of the proposed dual-band WPD and inset is the configuration of the WPD.

b. Step 2: Design of an RSRRM for WiMAX (3.5 GHz)

In the next step of the WPD design, the rectangular split ring resonator metamaterial is placed between the open circuit stubs. Although several kinds of resonators could have been employed in the design, we have chosen an RSRRM shown in Figure 4a. It should be noted that the area between open circuit stubs shown in Figure 3, is limited. So, a perfectly design that do not

increase the WPD size, is an important achievement. It is one of the most important features of our work. The equivalent circuit model for RSRRM structure is shown in Figure 4b, where C represents the TL capacitor, and the resonators are represented by the resonant tanks formed by C_{RSRRM} and L_{RSRRM} [25].

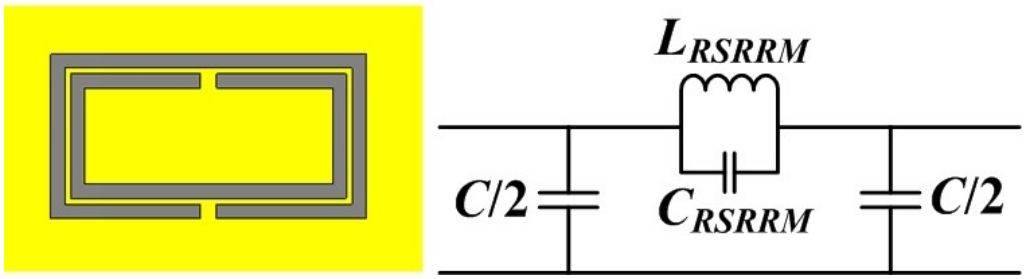

(a) (b)

Figure 4. (a) Configuration of the RSRRM structure and (b) its equivalent circuit model
Note: the area highlighted in yellow represents the ground-plane

The frequency of the transmission-zero (TZ) f_z is obtained by setting the admittance of the series branch to zero, namely:

$$Y_1 + Y_2 = j(\omega C_{RSRRM} - \frac{1}{\omega L_{RSRRM}}) = 0, \tag{3}$$

Thus, $$f_z = \frac{1}{2\pi\sqrt{L_{RSRRM} C_{RSRRM}}}. \tag{4}$$

The resonance frequency of RSRRM is given by:

$$f_r = \frac{1}{2\pi\sqrt{C(L_{RSRRM} + C_{RSRRM})}}. \tag{5}$$

In order to verify the proposed circuit model, the equivalent model presented in Figure 4b is simulated in the CST Design Studio 2017 software. To create a TZ and a resonance around 3.5 GHz, the values of L_{RSRRM}=259.8 pH, C_{RSRRM}=7.958 pF, and C=106.9 μF are obtained. The S_{11} and S_{21} parameters obtained from the CST Design Studio 2017 software are reported in Figure 5. It is observed that a resonance has been created at 3.5 GHz. Now, with the confirmation of the equivalent circuit model, a full-wave analysis is presented.

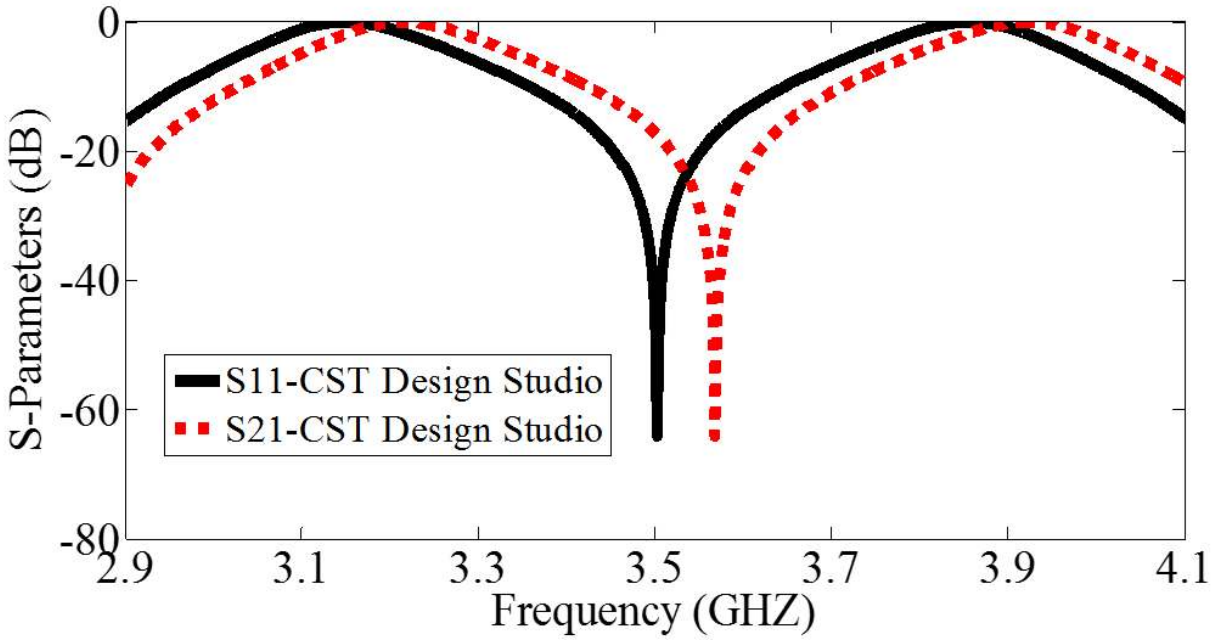

Figure 5. S_{11} and S_{21} parameters of the proposed circuit equivalent for RSRRM unit cell in CST Design Studio 2017.

The RSRRM structure inset in Figure 6a was designed based on equations in [21], where the geometric parameters are: A=15, B=10, a=7, b=13.5, c=0.35, d=0.6, and g=0.4 (all in millimeters). These parameters were determined for resonance close to the WiMAX frequency of 3.5 GHz. This design in addition to its desired frequency response (WiMAX application) could be embedded exactly in Π-shaped structure shown in Figure 3. Two waveguide ports are adjusted in the y-direction, and PMC as well as PEC boundaries are assigned in the xy and yz planes, respectively. The S_{11} and S_{21} response of the RSRRM unit cell structure are shown in Figure 6a. The transmission-minima is close to the desired frequency of operation. Note that the Figure 6a indicates a potential employment to design a filtering power divider. This condition is a natural performance of the metamaterial-based structures [26].

According to the design equations in [25], the relative permeability is extracted by using Equation (6), where β_0 is the wave number and h is the thickness of the substrate. The real and imaginary parts of the retrieved magnetic permeability are shown in Figure 6b.

$$\mu_r = \frac{2}{j\beta_0 h}\frac{1-(S_{12}-S_{11})}{1+(S_{12}-S_{11})}. \tag{6}$$

It is also clear that the usual parameter retrieval procedure is not directly applicable to single metamaterial unit cell due to the violation of periodicity. Nevertheless, the retrieved permeability provides a fair indication of the presence of metamaterial properties even at the single unit cell level.

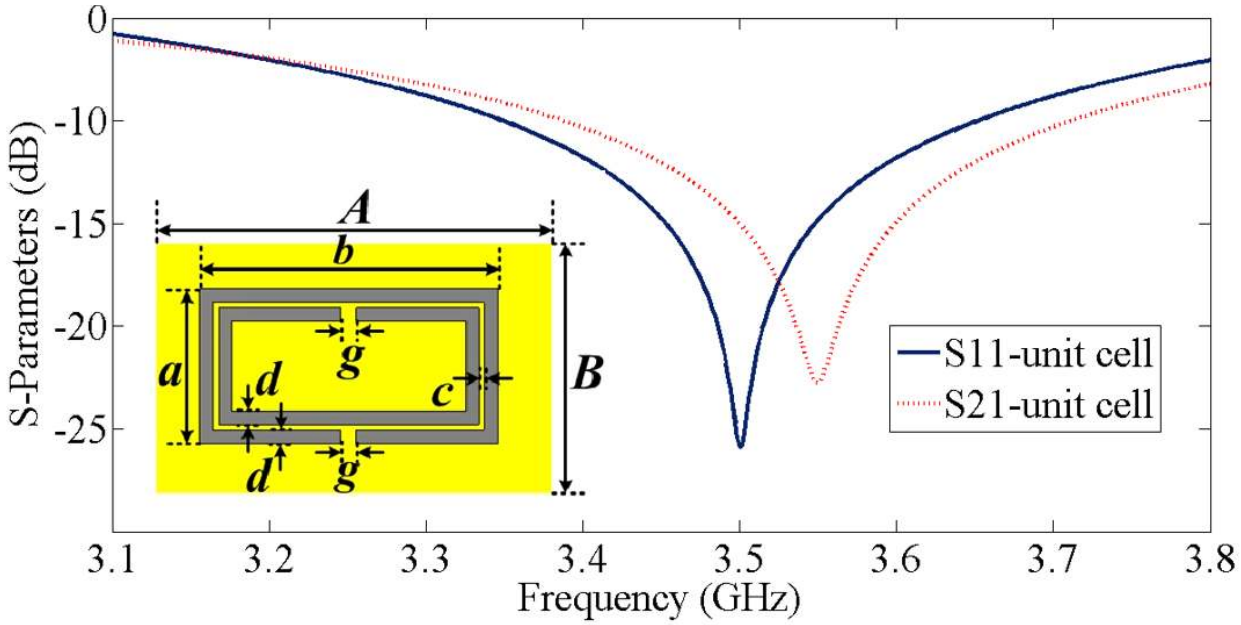

(a)

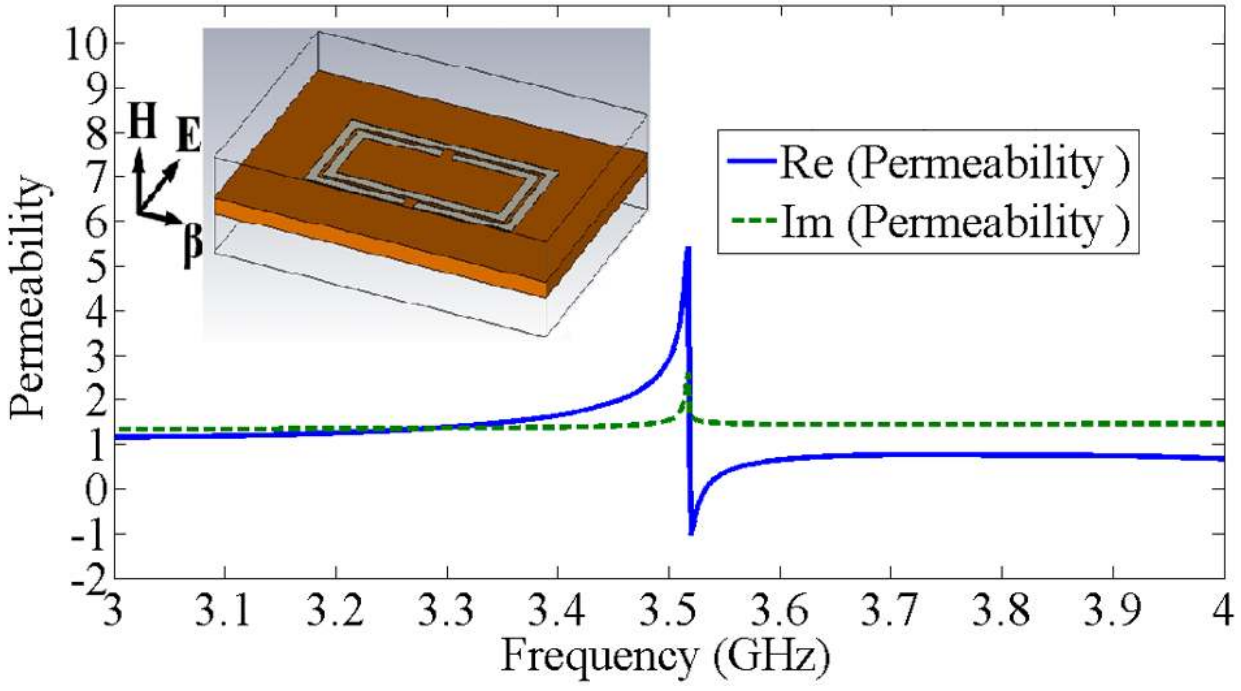

(b)

Figure 6. (a) S_{11} and S_{22} parameters for the RSRRM unit cell and unit cell configuration and (b) real and imaginary parts of retrieved permeability and inset is a 3-D view of the RSRRM unit cell.

c. Step 3: Constructing the Proposed RSRRM-WPD and Optimization

The designed RSRRM structure was placed between the open circuit stubs of the proposed dual-band WPD. Four cases are considered, as illustrated in Figure 7. The S_{11} and S_{21} responses for four cases are shown in Figures 8a and 8b, respectively. The effect of coupling between the proposed RSRRM and the WPD is also considered. This coupling is a function of the distance

between the RSRRM (m parameter) and the series TL (Z_2, θ_2) [24]. In cases (a) and (c), this distance is very small (m=0.35 mm), and in cases (b) and (d), this distance is large (m=3.5 mm). Thus, the S_{11} response is better than cases (b) and (d), because of the stronger coupling between RSRRM and the WPD structure [24]. The effect on the S_{11} response by the orientation of RSRRM structure is also considered. The orientation of RSRRM structure in cases (c) and (d) is identical, and the orientation in cases (a) and (b) are identical. From Figure 8 it is evident that the RSRRM-WPD structure in case (c) exhibits the best S_{11} (S_{11}<-30 dB) and S_{21} responses at 3.5 GHz. Hence, the structure in case (c) was chosen in the design of the proposed tri-band RSRRM-WPD.

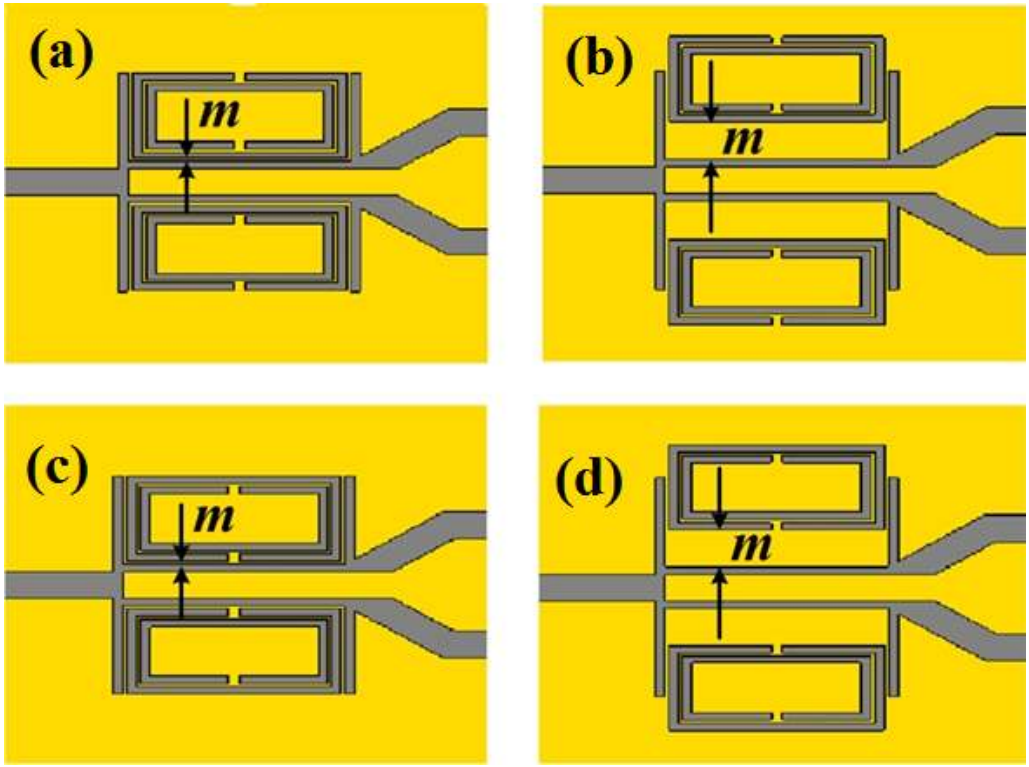

Figure 7. Four variants of the proposed RSRRM-WPD.

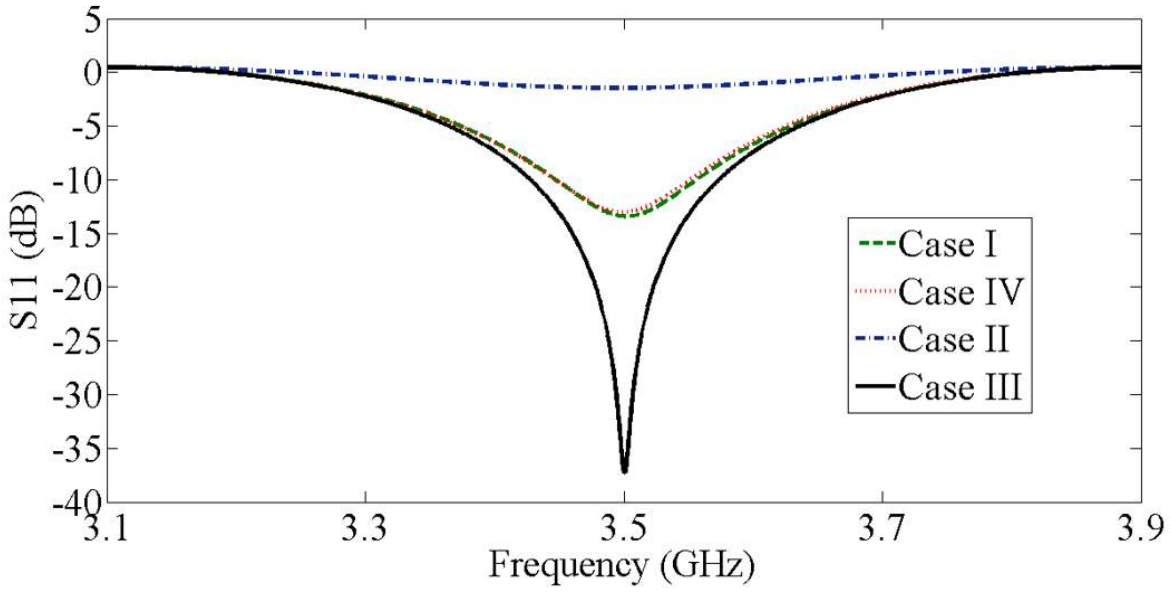

(a)

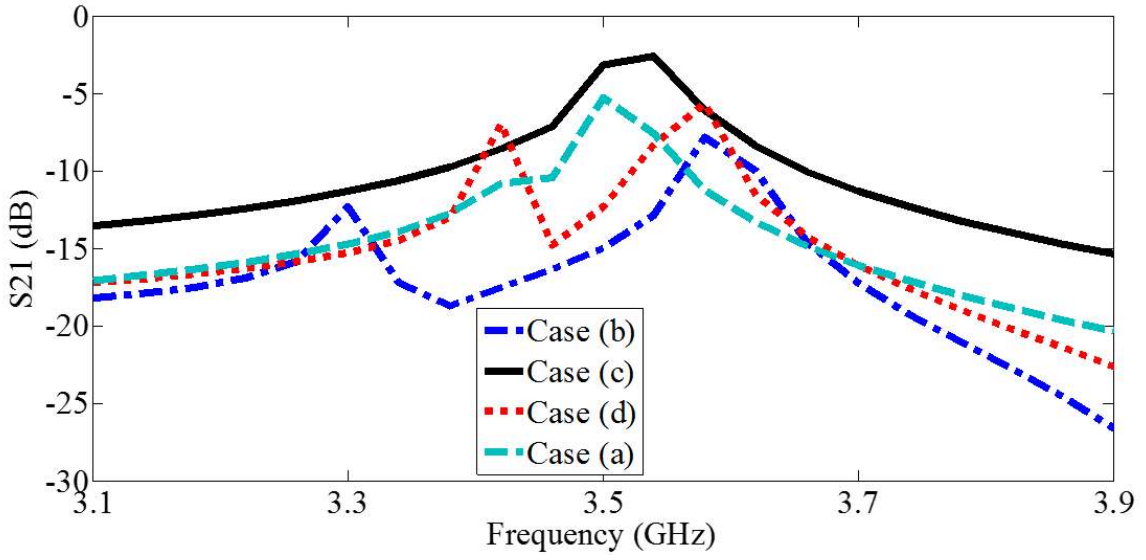

(b)

Figure 8. S_{11} and S_{21} responses of the four RSRRM-WPD structures presented in Figure 6 (a) S_{11} and (b) S_{21}.

Now, in order to achieve the optimal response by the CST Microwave Studio 2017 simulator, a parametric report is presented in Table 1. In Table 1, the effects of the *t* parameter on the resonance frequencies, return-loss, and insertion-loss are investigated. The *t* parameter is introduced in Figure 1. Due to the presence of the RSRRM in the vicinity of the Π-shaped structure and the existence of mutual coupling effects, the *t* parameter has been selected for frequency adjustment. According to Table 1, with the choice of t=4.6 mm, the operating frequencies are equal to 2.4 GHz, 3.5 GHz, and 5.2 GHz, as well as the most optimal frequency response for the S_{11} and S_{21} parameters.

In order to improve the frequency selectivity of the proposed RSRRM-WPD, an additional TZ is required which is adjacent to the passband. This is achieved by introducing an inter-

coupling structure in series with TL (Z_2, θ_2) between the input and output ports of the RSRRM-WPD, as described in [27]. This is implemented by etching a gap of size Gap between the input and output microstrip TL, as shown in the inset of Figure 1. The TZ is introduced close to the passband at f=2.75 GHz. Frequency resonances, TZ frequencies locations, and insertion-loss for different values of the Gap parameter, are presented in Table 2. It can be seen that with the increase of the Gap parameter from 0.1 mm to 1.5 mm, the location of the TZ is moved from 2.54 GHz to 3.14 GHz. Regarding the frequency responses, the optimized value of Gap is 0.6 mm. Also, in the last column of Table 2, a report of the stop-band created by TZ is presented in the frequency range of 2.5 to 3.5 GHz. It is seen that the above choice has a good frequency response condition.

Table 1. Resonance frequencies, return-loss, and insertion-loss for different values of *t*.

t **(mm)**	f_1 **(GHz)**	f_2 **(GHz)**	f_3 **(GHz)**	**Return-loss (S_{11}) (dB)**	**Insertion-loss (S_{21}) (dB)**
0.4	2.35	3.63	5.24	05.02/35.62/39.41	4.40/3.50/3.28
1.0	2.35	3.61	5.23	07.84/38.13/37.23	4.24/3.05/3.34
1.6	2.38	3.63	5.24	09.23/40.61/34.01	4.08/3.65/3.53
2.2	2.38	3.63	5.23	11.64/43.43/36.44	4.54/3.75/3.26
2.8	2.37	3.61	5.24	16.46/49.32/45.04	3.63/3.68/3.05
3.4	2.36	3.56	5.25	22.02/42.02/43.80	3.27/3.16/3.01
4.0	2.38	3.55	5.26	27.79/44.45/47.20	3.72/3.07/3.30
4.6	**2.40**	**3.50**	**5.20**	**35.63/47.28/52.06**	**3.21/3.03/3.04**
5.2	2.42	3.51	5.19	35.76/43.13/42.03	3.41/3.30/3.01
5.8	2.43	3.53	5.17	37.04/48.58/41.74	3.72/3.97/3.01
6.4	2.45	3.51	5.16	35.31/32.82/52.32	4.36/3.43/3.01
7.0	2.46	3.52	5.14	30.06/32.03/47.35	4.37/3.01/3.01
7.6	2.49	3.55	5.14	25.21/33.46/41.21	4.83/3.31/3.01
8.2	2.50	3.56	5.15	17.54/27.15/44.39	4.96/3.56/3.01

Table 2. The effect of Gap on the resonance frequencies, TZ frequency, and insertion-loss.

Gap (mm)	f_1 **(GHz)**	f_2 **(GHz)**	f_3 **(GHz)**	**TZ frequency (GHz)**	**Insertion-loss in TZ frequency (dB)**	**Stop-band created by TZ (GHz)**
0.1	2.41	3.53	5.24	2.54	56.90	0.72
0.2	2.41	3.53	5.21	2.57	54.52	0.75
0.3	2.40	3.53	5.23	2.60	57.14	0.82
0.4	2.40	3.51	5.20	2.64	58.04	0.79
0.5	2.40	3.52	5.20	2.69	59.33	0.84
0.6	**2.40**	**3.50**	**5.20**	**2.75**	**59.61**	**0.91**
0.7	2.41	3.53	5.19	2.79	59.09	0.90
0.8	2.40	3.50	5.20	2.83	54.13	0.78
0.9	2.40	3.52	5.19	2.87	56.45	0.83
1.0	2.41	3.54	5.19	2.89	47.29	0.71
1.1	2.40	3.51	5.18	2.93	43.17	0.57
1.2	2.40	3.50	5.18	2.99	41.02	0.79
1.3	2.40	3.50	5.18	3.06	38.78	0.81
1.4	2.40	3.52	5.19	3.11	38.03	0.76
1.5	2.40	4.50	5.18	3.14	36.27	0.83

3. Experiment Results and Discussion

The proposed RSRRM-WPD was fabricated to determine the accuracy of the design and simulated results. The measured and simulated S-parameters of the proposed RSRRM-WPD are shown in Figure 9. The discrepancy between the simulated and measured results of 1.3% is attributed to the manufacturing tolerance. The three passbands are centered at 2.4, 3.5, and 5.2 GHz, with the fractional bandwidths of 3.86%, 5.82%, and 3.89%, respectively. The measured return-loss (S_{11}) at the center frequency of the three passbands is better than 40 dB, and the corresponding insertion-loss (S_{21}) is better than 4 dB. The measured isolation between the output ports (S_{23}) is 27 dB at 2.4 GHz, 39 dB at 3.5 GHz, and 28 dB at 5.2 GHz.

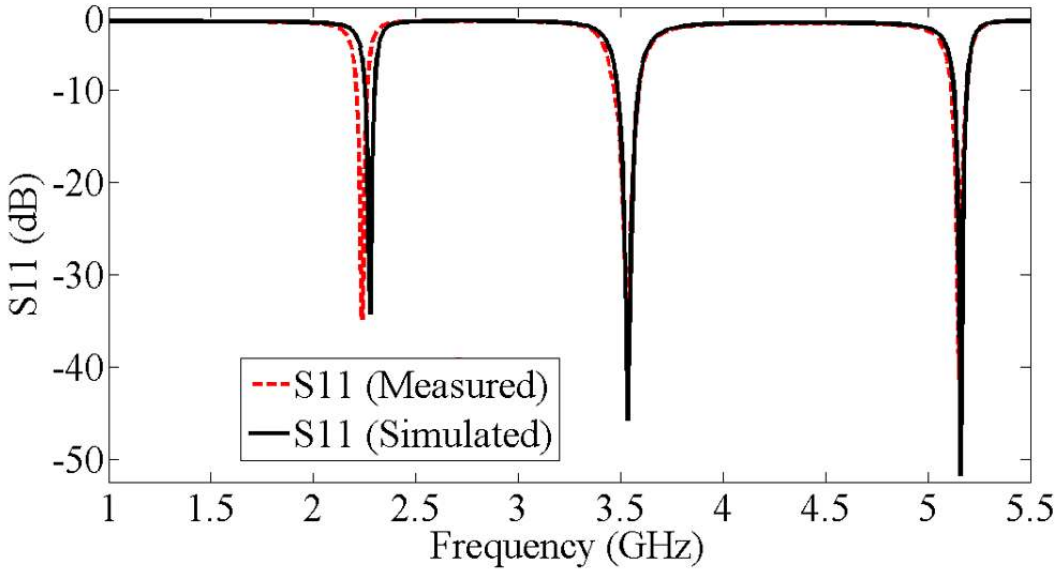

(a)

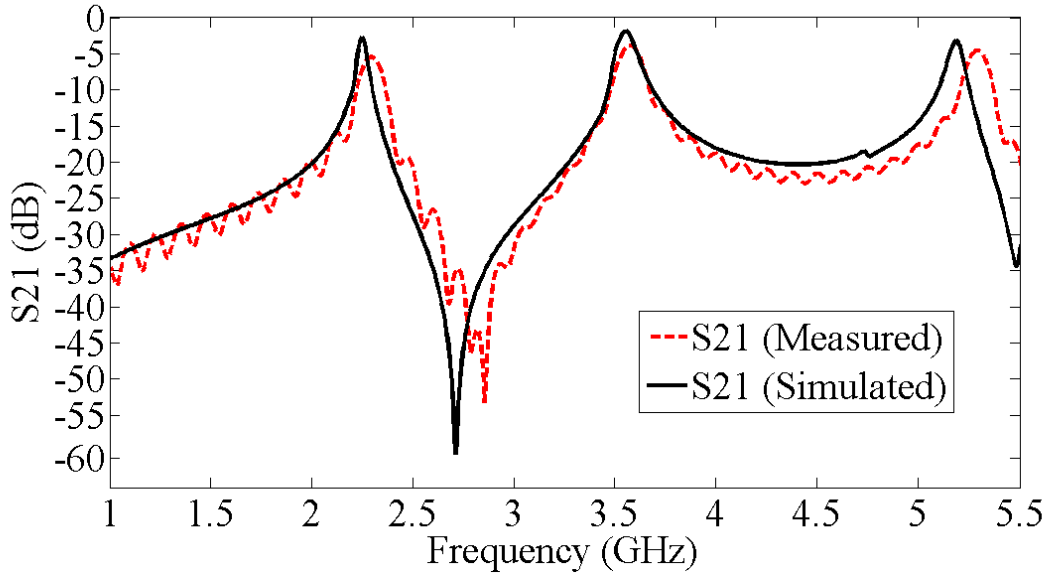

(b)

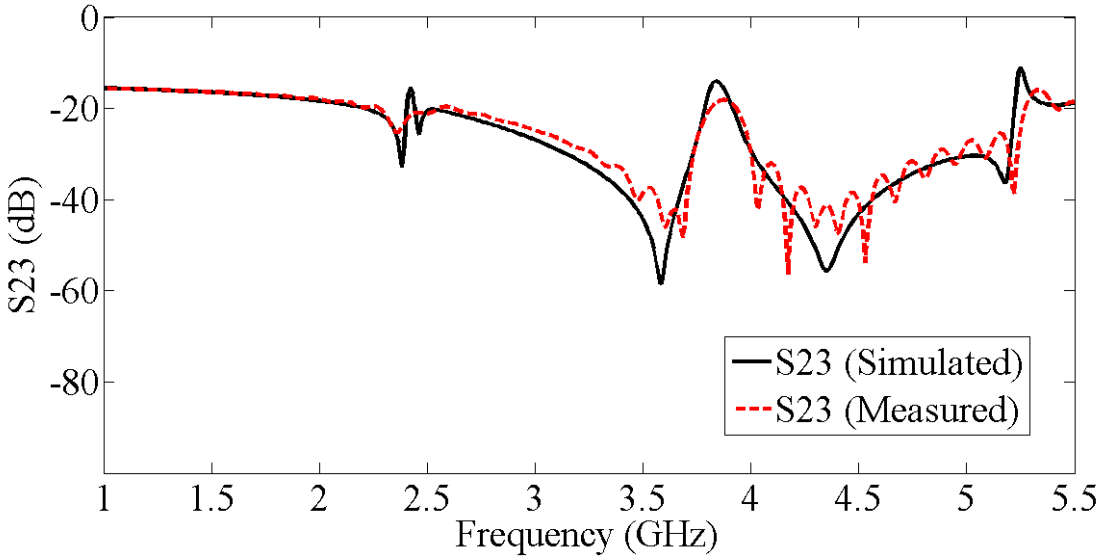

(c)

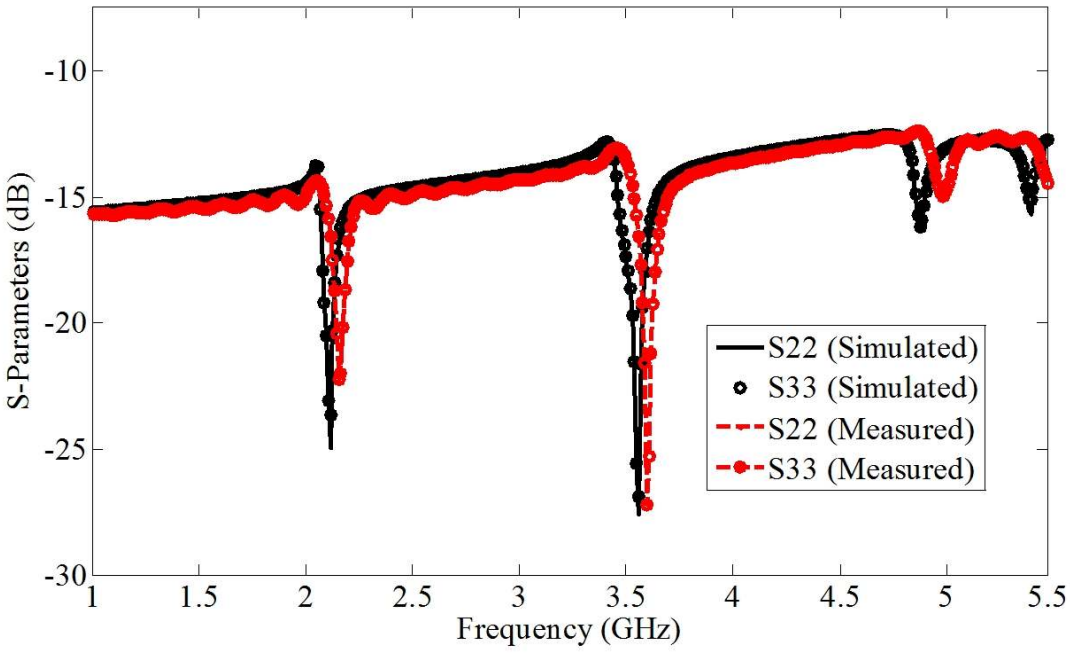

(d)

Figure 9. Simulated and measured S-parameters of the propose RSRRM-WPD (a) S_{11} (b) S_{21} (c) S_{23} (d) S_{22}, and S_{33}.

Also, magnitude and phase difference is shown in Figure 10a and Figure 10b, respectively. The in-band amplitude imbalance is less than 0.15 dB. In addition, the measured phase difference is about ±1.5°. It indicates a very good in-phase performance. A photograph of the fabricated structure is shown in Figure 11. The dimensions of the power divider are 14×17.9 mm^2 or $0.15\lambda_g \times 0.19\lambda_g$, where λ_g is the guided wavelength of at f_1=2.4 GHz. The measurements on the device were conducted using Agilent network analyzer HP8722ES. Table 3 shows the proposed RSRRM-WPD in comparison with prior dividers.

The following is a report on comparing the proposed WPD with other previous designs. According to Table 3, the overall dimensions of the structure introduced in reference [9] are 0.754 λ_g^2. So, the dimensions of our design have decreased by more than 30%. On the other hand, on average The isolation of the proposed WPD with the PD presented in reference [9], is at a level. The dimensions of our design have diminished by 10% compared to the WPD reported in [14]. But more importantly, the conditions for the isolation and return-loss of the proposed WPD are better than the PD in reference [14]. It can also be argued, for example, that the proposed WPD, compared to the structure introduced in reference [21], is only slightly smaller in size, but the conditions for isolation and insertion-loss are more appropriate. Note that lumped-elements are used in the design of the structure which presented in [21]. This has reduced the size of the structure. At the end, it shows that the proposed WPD is one of the smallest structures presented to date which is 60% smaller than conventional design [5]. The characteristics of the WPD make the device suitable for use in Bluetooth, WLAN, and WiMAX systems.

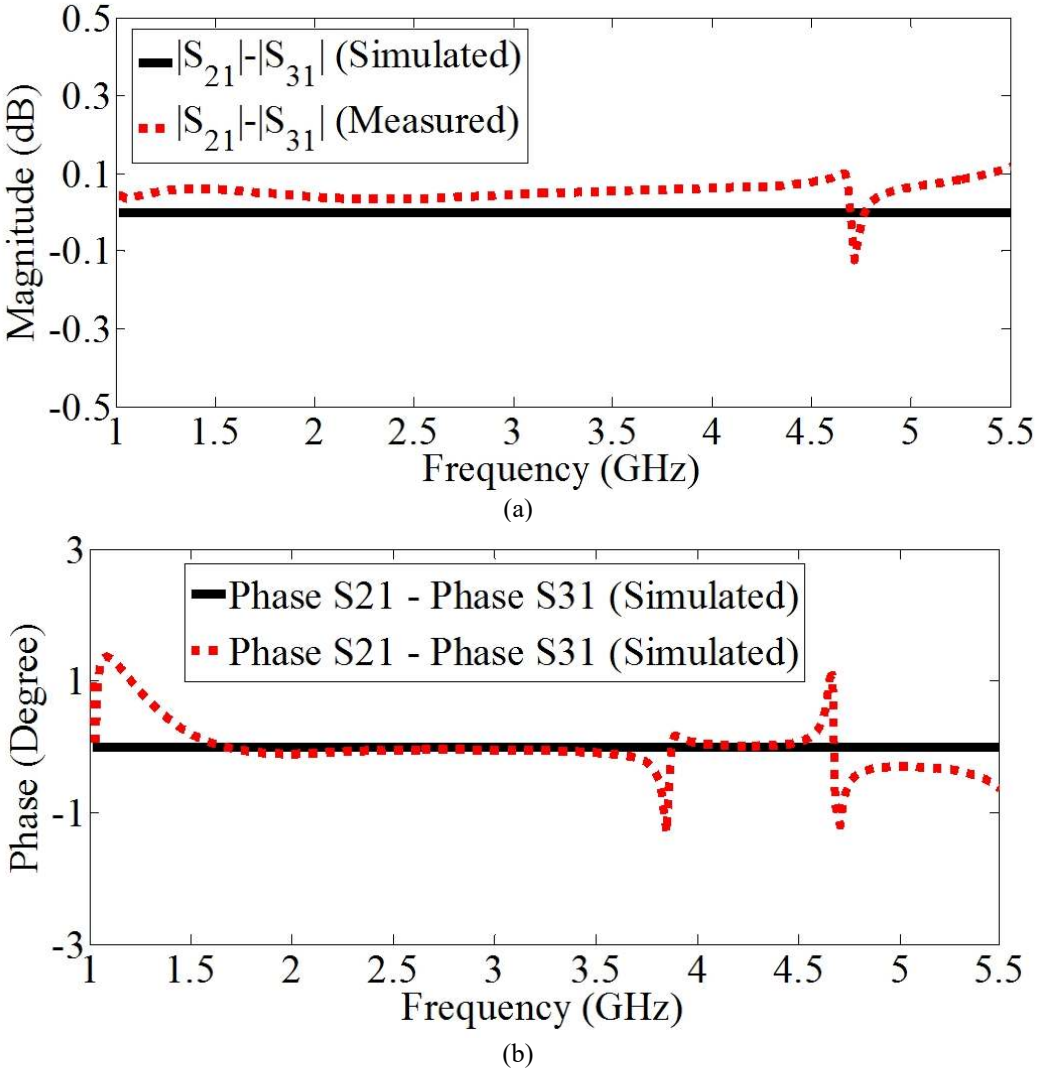

Figure 10. Simulated and measured performance of the proposed RSRRM-WPD (a) Magnitude difference and (b) phase difference.

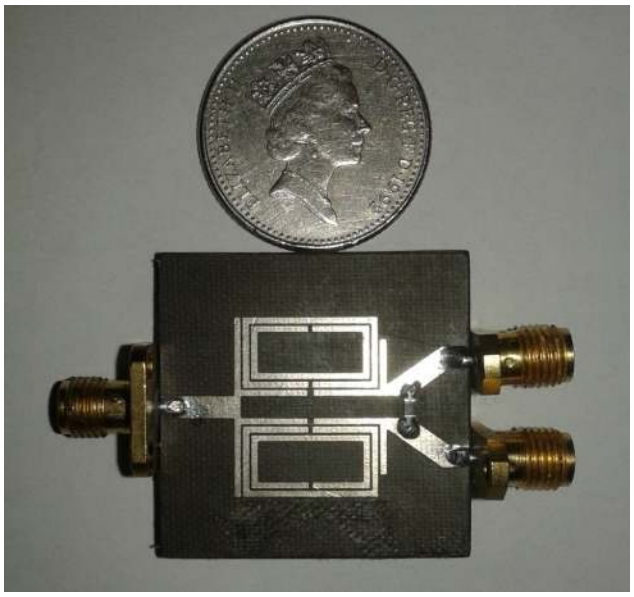

Figure 11. Photograph of the proposed RSRRM-WPD.

Table 3. Performance comparison of this work with other power dividers.

Ref.	Substrate Height (mm)/ε_r	Pass-bands (GHz)	Return-loss (dB)	Insertion-loss (dB)	Isolation (dB)	FWB (%)	Circuit Size ($\lambda_g \times \lambda_g$)/(mm^2)
[5]	1.57/3.45	0.9/1.17/2.43	35/31/26	3±0.4	37/30/20	---	0.56×0.34/1705
[8]	1.965/5	0.7/1.96	>30/>30	3±1	>30/>30	71.43/25	0.46×0.1/300
[9]	0.76/2.94	0.92/2.45/5.8	>16/>16/>16	3±2	>27/>33/>23	---	0.2×3.77/396
[14]	0.785/3.48	1.5/1.9/2.35	23/19/20	3±1.5	>15>15>15	40/10.5/17.9	---/2508
[20]	1.524/3.38	0.8/1.3/1.8	49.8/41.4/28.9	3±2	23.3/25.1/29	14.7/12.5/6.5	0.66×0.16/1444
[21]	1.524/3.55	2.45/5.2	25/20	3±2	27.5/19.2	17.5/26	0.2×0.2/---
[22]	1.5/2.2	1.9/6.6	>10/>10	3±2	>15/>15	94.2/12.9	1.77×2/555
This work	**0.8/2.65**	**2.4/3.5/5.2**	**42/49/52**	**3±1**	**27/39/28**	**3.86/5.82/3.89**	**0.15×0.19/250**

4. Conclusion

A highly compact and novel tri-band WPD structure has been presented, which was realized by substituting the quarter-wavelength TL in the WPD design with a Π-shaped TL coupled to an RSRRM structure. Compared with the previous power dividers, the proposed design offers a miniature size. The simulation and measured results have confirmed the device exhibits excellent insertion-loss, return-loss, and isolation characteristics. The tri-band device covers frequency bands of Bluetooth (2.4 GHz), WiMAX (3.5 GHz), and WLAN (5.2 GHz).

References

[1] Pozar DM. Microwave engineering. 4th ed. New York (NY): Wiley; 2012.

[2] Wu L, Yilmaz H, Bitzer T, Berroth M. A dual-frequency Wilkinson power divider: for a frequency and its first harmonic. IEEE Microwave Wirel. Compon. Lett. 2005;15:107-109.

[3] Wu L, Sun Z, Yilmaz H. A dual-frequency Wilkinson power divider. IEEE Trans. Microwave Theory Tech. 2006;54:278-284.

[4] Zhang T, Che W, Chen H, Feng W. A compact four-way dual-band power divider using lumped elements. IEEE Microwave Wirel. Compon. Lett. 2015;25:94-96.
[5] Chongcheawchamnan M, Patisang S, Krairiksh M, Robertson ID. Tri-band Wilkinson power divider using a three-section transmission-line transformer. IEEE Microwave Wirel. Compon. Lett. 2006;16:452-454.
[6] Xia B, Wu LSh, Mao J, Yang L. A new quad-band Wilkinson power divider. J. Electromagn. Waves App. 2014;28:1622-1634.

[7] Cheng KKM, Wong FL. A new Wilkinson power divider design for dual band application. IEEE Microwave Wirel. Compon. Lett. 2007;17:664-666.
[8] Wang X, Sakagami I, Ma Z, Mase A, Yoshikawa M, Ichimura M. Miniaturized dual-band Wilkinson power divider with self-compensation structure. IEEE Trans. Compon. Packag. Manuf. Tech. 2015;5:389-397.
[9] Wu Y, Shen J, Liang L, Wang W, Liu Y. A novel compact tri-band Wilkinson power divider based on coupled lines. Electromagnetics. 2013;33:59-72.
[10] Hu Sh, Song K, Fan Y. Multilayer four-way power divider with improved isolation performance. J. Electromagn. Waves App. 2017;31:1676-1684.

[11] Ahmed UT, Abosh AM. Design of wideband single-layer in-phase power divider using microstrip to slotline coupled structure. Microwave Opt. Technol. Lett. 2015;57:789-791.
[12] Dadgarpour A, Dadashzadeh G, Naser-Moghadasi, Jolani F, Virdee BS. PSO/FDTD optimization technique for designing UWB in-phase power divider for linear array antenna application. IEEE Antennas Wirel. Propag. 2010;9:424-427.
[13] Ahmed UT, Abosh AM. Extremely wideband in-phase power divider using modified Wilkinson design. Microwave Opt. Technol. Lett. 2015;57:1799-1802.
[14] Abdelrahman BM, Ahmed HN, Nashed AI. A novel tri-band Wilkinson power divider for multiband wireless applications. IEEE Microwave Wirel. Compon. Lett. 2017;27:891-893.
[15] Chang CL, Tseng CH. Compact Wilkinson power divider using two-section asymmetrical T-structures. Electron. Lett. 2013;49:546-547.
[16] Du ZX, Zhang XY, Wang KX, Kao HL, Zhao XL, Li XH. Unequal Wilkinson power divider with reduced arm length for size miniaturization. IEEE Trans. Compon. Packag. Manuf. Tech. 2016;6:282-289.

[17] Mirzavand R, Honari MM, Abdipour A, Moradi GR. Compact microstrip Wilkinson power dividers with harmonic suppression and arbitrary power division ratios. IEEE Trans. Microwave Theory Tech. 2013;61:61-68.
[18] Guo Z, Yang Y. A novel compact Wilkinson power divider with controllable harmonic suppression and simple structure. J. Electromagn. Waves App. 2018;32:601-608.
[19] Li Q. Zhang Y. Wu CTM. High-selectivity and miniaturized filtering Wilkinson power dividers integrated with multimode resonators. IEEE Trans. Compon. Packag. Manuf. Tech. 2017;7:1990-1997.

[20] Genc A. Baktur R. Dual- and triple-band Wilkinson power dividers based on composite right- and left-handed transmission lines. IEEE Trans. Compon. Packag. Manuf. Tech. 2011;1:327-334.
[21] Zhang HL, Hu BJ, Zhang XY. Compact equal and unequal dual-frequency power dividers based on composite right-/left-handed transmission lines. IEEE Trans. Indust. Electron. 2012;59:3464-3472.
[22] Wu GC, Wang G, Sun JJ, Gao XJ, Wang YW. Compact dual-band power divider based on dual composite right/left-handed transmission line. Electron. Lett. 2014;50:759-761.
[23] Shuai Y, Deng H. Novel balanced composite right-/left-handed unit and its application in multiband power divider. Microwave Opt. Technol. Lett. 2017;59:1100-1107.
[24] Khajeh-Khalili F, Honarvar MA. A design of triple lines Wilkinson power divider for application in wireless communication systems. J. Electromagn. Waves App. 2016;30:2110-2124.
[25] Khajeh-Khalili F, Honarvar MA. Novel tunable peace-logo planar metamaterial unit-cell for millimeter-wave applications. ETRI J. 2018;40:389-395.

[26] Ketzaki DA, and Yioultsis TV. Metamaterial-based design of planar compact MIMO monopoles. IEEE Trans. Antennas Propag. 2013;61:2758-2766.

[27] Chen FC, Hu HT, Li RS, Chu XQ, Lancaster MJ, Design of filtering microstrip array with reduced sidelobe level. IEEE Trans. Antennas Propag. 2017;65:903-908.